*RIMS Kôkyûroku Bessatsu*
**B31** (2012), 167–194

# Refraction, Reflection and Splitting

*With thanks to all the people who allowed us to continue to make a research.*

By

Yasumasa NISHIURA* and Takashi TERAMOTO**

## Abstract

We discuss the behaviors of traveling 2D spots arising in a three component reaction diffusion system when the media has a jump heterogeneity along the line. The traveling spot responds in various ways depending on the the height of the jump and the incident angle when it encounters the jump line. Refraction and reflection are commonly observed. Two issues are discussed here: One is the relation between the incident angle and the refraction angle when the spot crosses the jump. In a scaling limit near a drift bifurcation, a Snell's-like law holds for the refraction case. The other is the transition from refraction to reflection. Such a transition occurs as the incident angle is increased for a fixed height or the height is increased for a fixed incident angle. As the angle (or height) approaches the critical one, the spot spends much longer time in the right half plane after crossing the jump line and it eventually converges to the one traveling parallel to the jump line but infinitely far from it, namely it is a traveling spot in the homogeneous space located at right infinity. We call such a special solution "scattor" located at infinity. Since such a scattor was found originally for collision dynamics in which its role is exemplified nicely, a short review is given before discussing the behaviors in heterogeneous media. An interesting thing is that most of the scattors are common both in the collision and heterogeneous problems, in fact we take a traveling peanut solution as a typical example, which controls the transition between merging and splitting.

## § 1. Introduction

Spatially localized dissipative structures are observed in various fields such as chemical reactions, discharge patterns, morphological dynamics, granular materials, and binary

Received December 8, 2011. Revised January 6, 2012.
2000 Mathematics Subject Classification(s): 34C20, 35B32, 35B36, 35K57
*Key Words*: *reaction-diffusion equations, global bifurcation, dissipative soliton, collision dynamics, heterogeneous media*
*Research Institute for Electronic Science, Hokkaido University, Sapporo 060-0812, Japan.
Present address: WPI Advanced Institute for Materials Research Tohoku University Sendai 980-8577 Japan
e-mail: nishiura @ wpi-aimr.tohoku.ac.jp
**Chitose Institute of Science and Technology, Chitose 066-8655, Japan.
e-mail: teramoto@photon.chitose.ac.jp

convection [1, 2, 3, 4, 8, 11, 12, 15, 16, 32, 39, 41, 42]. Those patterns are much simpler than a single living cell, however they seem to inherit several characteristic features of *living state*, for instance, self-replication and self-destruction can occur without any external trigger [5, 13, 9, 17, 26, 27, 29]; a variety of deformations at collisions [20, 21, 22, 35, 36]; adaptive behaviors depending on external environments and heterogeneities [33, 34, 40]. These behaviors come from the interplay between a variety of internal dynamics of each localized pattern and the external triggers and environmental changes such as collisions and spatial-temporal heterogeneities in the system.

Although there are many important problems from single motion to coherent behaviors related to spot dynamics, we have been interested in two main issues: one is the collision dynamics and the other is the motion of traveling pulses and spots in heterogeneous media. Since they are moving, it is unavoidable for them to collide each other or meet the heterogeneities. The main difficulty of the first issue is two-fold: one is how we can describe the large deformation at collision, the other is to find the underlying mechanism controlling input-output relation. It has been uncovered that large deformation at collision is mapped into the network of unstable patterns called **scattors** [20, 21, 22, 35]. Namely large deformations can be translated into the heteroclinic connections in the network. We shall give a quick survey on this issue in Section 3 and try to explain how such a network becomes a backbone for large deformations at collisions. We also show a traveling localized spot of peanut shape as a representative example of scattor. As for the second issue, it is about the interaction between moving objects and the surrounding environments, in particular, how spatial heterogeneities affect the motion of traveling pulses and spots, which may be regarded as a kind of collision problem between them. Even for the simple class of heterogeneity such as jump or bump shape, the traveling objects can display a variety of dynamics after hitting the jump including pinning and splitting as well as transmission and reflection [18, 24, 25, 28, 36, 43, 46]. This is mainly due to the fact that the heterogeneity becomes a trigger for the emergence of instabilities hidden in the localized patterns.

The main issue in this paper is to study the behaviors of traveling spots in the heterogeneous media, especially focus on the simplest case; a jump discontinuity along the line. Figure 1 shows typical behaviors of traveling spots as the height of the jump is gradually increased with the incident angle $\theta_i$ being fixed to $\pi/4$. Here we employ the model system (2.1) in Section 2 for the computation. When the height is low, it can go over the jump, but **refraction** occurs as in Figs.1(a)(b) because of the difference of velocities on both sides. As the height exceeds a critical level, the spot bends back and **reflection** occurs. The same thing could happen when the incident angle is increased with the height being fixed. Two natural questions arise here.

1. When transmission occurs, what is the relation between the incident angle $\theta_i$ and

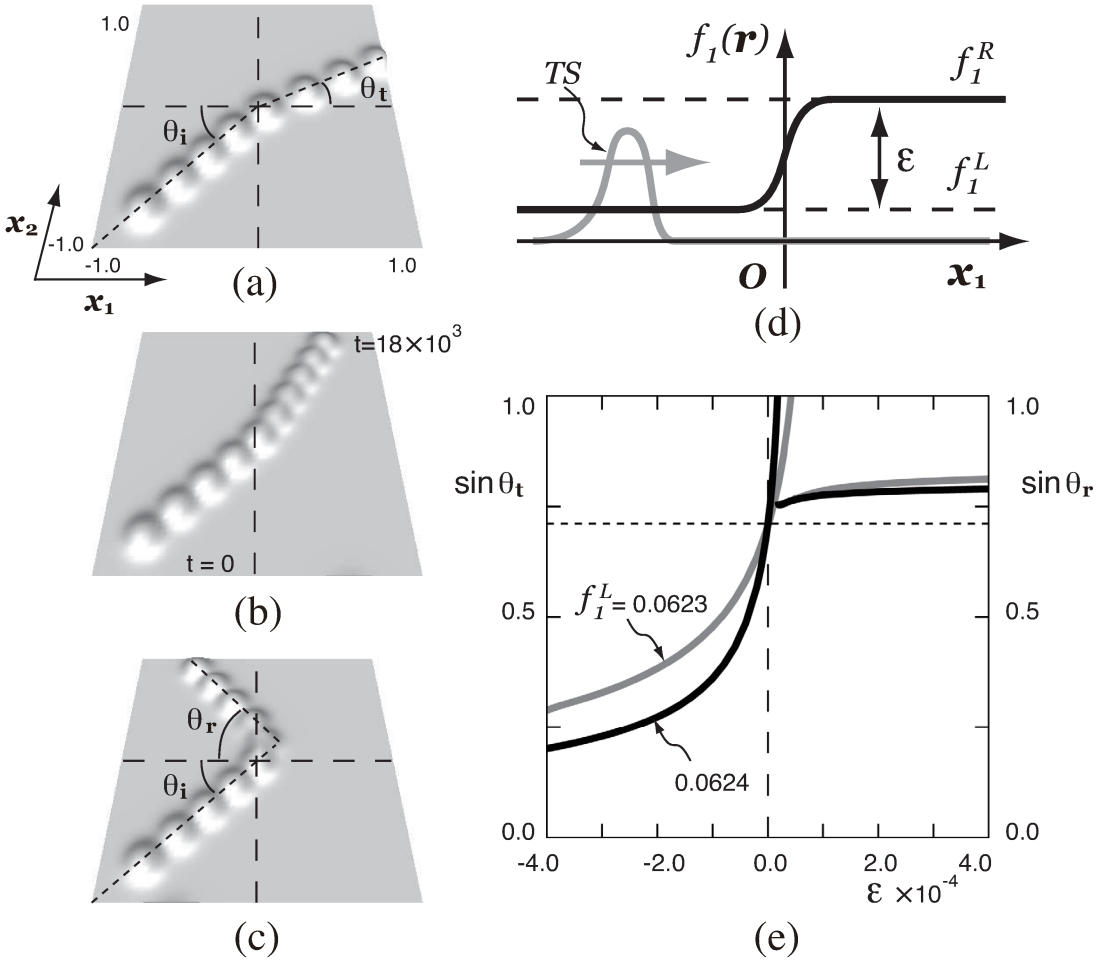


Figure 1. Refraction and reflection behaviors of the traveling spots encountering the jump heterogeneity. Time evolutions of oblique collisions for (2.1) with $f_1^L = 0.0623$, $\theta_i$ being fixed to $\pi/4$ and the vertical broken line indicating the location of jump line. (a)(b) Refraction: trajectories of spot motion bend away and towards from the perpendicular for $\epsilon = 3 \times 10^{-5}$ and $-1.2 \times 10^{-4}$, respectively, (c) Reflection for $\epsilon = 6.0 \times 10^{-5}$. (d) Schematic picture shows a manner how a traveling spot hits jump-type heterogeneity from left side. Solid line shows how $f_1(\boldsymbol{r})$ spatially changes in the $x_1$ direction. (e) The $\epsilon$-dependence curves of the refraction and reflection angle, $\theta_t$ and $\theta_r$, for $f_1^L = 0.0623$ and 0.0624 are indicated by gray and solid lines, respectively.

the refraction angle $\theta_t$?

2. When the transition from transmission to reflection occurs, what is the separatrix in between and how it controls the dynamics?

In order to characterize the velocities of traveling spots on both sides of the jump line, we resort to a reduction method from PDEs to ODEs near a supercritical drift bifurcation

in Section 4, which allows us to compute those quantities and study the change of angles around the heterogeneity. It turns out that a reverse type of the Snell's-like law holds for the first question.

To answer the second problem, it is necessary to introduce the two homogeneous spaces located at $\pm\infty$ taking a uniform value $f_1^L$ or $f_1^R$, respectively. It turns out that traveling patterns in those homogeneous spaces play a key role to understand such a transition and this is also the case for many other transitions including merging-splitting transition in Section 5. We will see that heteroclinic orbits naturally appear at the transition point, each of which connects two scattors living in those homogeneous spaces located at $\pm\infty$. A key message is to see that **a network structure consisting of heteroclinc orbits connecting various types of scattors** play a key role to resolve both collision and heterogeneous problems. Also note that exactly the same type of patterns such as traveling peanut one plays as a scattor in both problems.

## § 2. MODEL

In this paper we employ the following three-component reaction diffusion equations as an representative model for the study of collision problem and the dynamics in heterogeneous media. It is known that such a class of three-component systems supports stable traveling spots in higher dimensional space.

$$\begin{cases} u_t &= D_u\nabla^2 u - \dfrac{uv^2}{1+f_2 w} + f_0(1-u) \\ v_t &= D_v\nabla^2 v + \dfrac{uv^2}{1+f_2 w} - (f_0+f_1)v \\ \tau w_t &= D_w\nabla^2 w + f_3(v-w)\ . \end{cases} \tag{2.1}$$

The system (2.1) consists of the substrate $u = u(t, \boldsymbol{r})$, activator (or consumer) $v = v(t, \boldsymbol{r})$ and inhibitor $w = w(t, \boldsymbol{r})$ in two-dimensional space $\boldsymbol{r} = (x_1, x_2)$, where $(f_0, f_1, f_2, f_3)$, the diffusion coefficients $(D_u, D_v, D_w) = (2.0\times10^{-4}, 1.0\times10^{-4}, 5.0\times10^{-4})$, and $\tau$ are positive constants. If $w \equiv 0$, the system is reduced to the Gray-Scott model [7]. Note that H. Meinhardt already proposed the similar equations to (2.1) to describe the shell patterns [14]. We employ the following values for the other parameters as $f_0 = 0.05$, $f_2 = 0.50$, and $f_3 = 0.20$. The $f_1$ and $\tau$ are set to control parameters. For instance, we set $\tau = 40$ for refraction-reflection problem of Fig.1, since the drift bifurcation from standing spot to traveling one becomes supercritical, which fits our framework of reduction in Section 4.

## § 3. LARGE DEFORMATION AT COLLISION AND NETWORK OF UNSTABLE PATTERNS

Collision dynamics has been remained as an uncultivated area due to the complexity and large deformation of colliding objects. Although it is still a difficult task to describe all the aspects of the deformation, the network structure of the unstable patterns called *scattors* relevant to collision process plays a key role to clarify the backbone of large deformation process. Heteroclinic connections from high-codimension scattors to lower ones tell us how the deformation evolves after collision. It is clear that if initial and final states are different and stable at least locally, then the orbit in between must cross the basin boundaries. Collisions trigger the basin switching via large deformation. The aim of this section is to give a quick survey of recent development of collision dynamics of traveling spots. It turns out that those scattors are also relevant to the dynamics in heterogeneous media.

### § 3.1. HOW TO SET UP THE PROBLEM

One of the main questions for the collision dynamics is that how we can describe the large deformation of two localized objects at collision and predict its output. The strong collision usually causes topological changes such as merging into one body or splitting into several parts as well as annihilation. It is in general quite difficult to trace the details of the deformation unless it is a very weak interaction. We need a change in our way of thinking to solve this issue. So far we may stick too much to the deformation of each localized pattern and become shrouded in mystery. We try to characterize the hidden mechanism behind the deformation process. It may be instructive to think about the following metaphor: the droplet falling down the landscape with valleys and ridges as in Fig.2 (see also [45]). The motion of droplets on a rugged landscape is rather complicated; two droplets merge or split at the saddle points and they may sink into the underground, i.e., annihilation. On the other hand, the profile of the landscape remains unchanged and in fact controls the behaviors of droplets. It may be worth to describe the landscape itself rather than deformation: where is a ridge or a valley, and how they are combined to form a whole landscape. Such a change of viewpoint has been proposed by [20, 21, 22, 35] (see also [17]) claiming that the network of unstable patterns relevant to the collision process constitutes the backbone structure of the deformation process, namely the deformation is guided by the connecting orbits among the nodes of the network. Each node is typically an unstable ordered pattern such as steady state or time-periodic solution. This view point is quite useful and valid to various problems including the heterogeneous problems in Section 4.

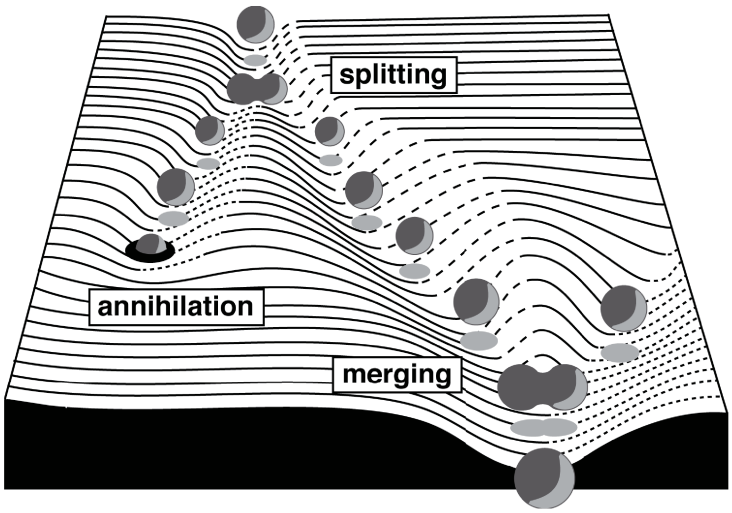


Figure 2. Droplets falling the rugged landscape. They merge or split depending on the local shape. They move around in a complicated way and deform largely when they meet other droplets, however the profile of the landscape, which does not change during the collision process, basically controls the dynamics of collisions.

## § 3.2. HEAD-ON COLLISION

In order to observe collision phenomena, the system (2.1) has to have stable traveling spots moving in different directions. One of the analytical methods for that purpose is to find a drift bifurcation point for standing spots, in fact there is a light gray "standing" region in Fig.3(a), in which stable standing spots exist. When the parameters $(f_1, \tau)$ cross the dotted solid line in the left-upward direction, stable traveling spots emerge supercritically, namely the dotted solid line is a drift bifurcation line above which stable traveling spots exist. We first consider the head-on collisions, i.e., two traveling spots approach along the line connecting the two centers of mass. Note that left-right and up-down symmetries hold for head-on case, however up-down symmetry is not preserved for the oblique case. There are three different outputs depending on the parameters as in Fig.3(a): RE (reflection), FD (fusion and drift), and AN (annihilation) [22]; FD, for instance, means that two spots merge into one body and become a disk of circular shape, then start to move in one-direction due to the drift instability. One may wonder that the circular spot after merging should not move in one direction due to the preservation of symmetry for head-on case. This is simply because there always exist numerical errors or noise that breaks the symmetry. It seems natural that two colliding spots reflect each other (i.e., the output belongs to RE regime) right after the drift bifurcation, since their velocities are small and interact weakly. Note that when the parameter close to the double critical point DH (the drift and Hopf instabilities), the dynamics becomes much

more delicate and annihilation occurs even if the velocity is small (the thick vertical dashed line in Fig.3(a) indicates the Hopf instability for large standing disk (SD) spot).

The main question here is to clarify the underlying mechanism for the transition I from RE to FD, or the transition II from FD to AN in Fig.3(a). Here we only consider the case near the boundary between RE and FD. As two traveling spots collide, they form a peanut shape with two peaks, then the middle part of the two peaks either grows or decays depending on the parameter set $(f_1, \tau)$ being in either FD or RE. Namely the peanut shape is a kind of separator controlling the output, in fact there is an unstable steady state of peanut shape depicted in Fig.3(c), which can be detected by the Newton method. The unstable manifold associated with the largest real eigenvalue of the standing peanut (SP) pattern is connected to the large SD and splitting into two traveling spots (TSs) moving in the opposite directions, depending on the sign of perturbation. Such a separator is called the *scattor* introduced by [20, 21]. When the parameter belongs to FD, the profile of orbit becomes very close to the large SD after peanut shape of SP, however it is not the final destination, since it still keeps a drift instability, therefore it eventually starts to move in one direction as mentioned before. A schematic diagram for the transition from RE to FD is shown in Fig.3(b), in which two scattors of SP and large SD appear and one of the unstable manifolds of SP is connected to the stable manifold of large SD. The transition from RE to FD occurs, when the orbit crosses the stable manifold of SP from below to above in Fig.3(b). There are three different types of scattor for head-on collision case: SP pattern, large SD, and small SD. These three scattors play a role of separators among RE, FD, and AN outputs as in Fig.3(c). It should be emphasized that the network of scattors connected by their unstable manifolds constitutes a backbone structure responsible for large deformation at collision. See [22] for more detailed discussions.

## § 3.3. OBLIQUE COLLISION

When collision occurs, it is generically an oblique one, i.e., it breaks at least up-down symmetry. We consider a class of oblique collisions in which left-right symmetry is preserved, namely it is equivalent to the case when the traveling spot hits the boundary under the Neumann boundary condition. The incident angle $\theta_i$ is varied as a parameter besides $f_1$. See Fig.4(c), in which $\tau$ is fixed to 90 and we study the spot behaviors near the transition II between FD and AN regimes in the phase diagram of Fig.3(a). Those head-on collisions are associated with the case of $\theta_i = 0^\circ$ in Fig.4(c). Note that RE (reflection) regime appears besides FD and AN regimes for large incident angles. If $\theta_i$ is increased and approaches $\pi/2$, it becomes closer to a parallel motion, therefore the reflection (RE) is possible and becomes dominant for larger incident angles as in the phase diagram of Fig.4(c). In the next subsection we study the transition III between RE and FD and find a new type of scattor for the oblique case of $\theta_i \neq 0^\circ$.

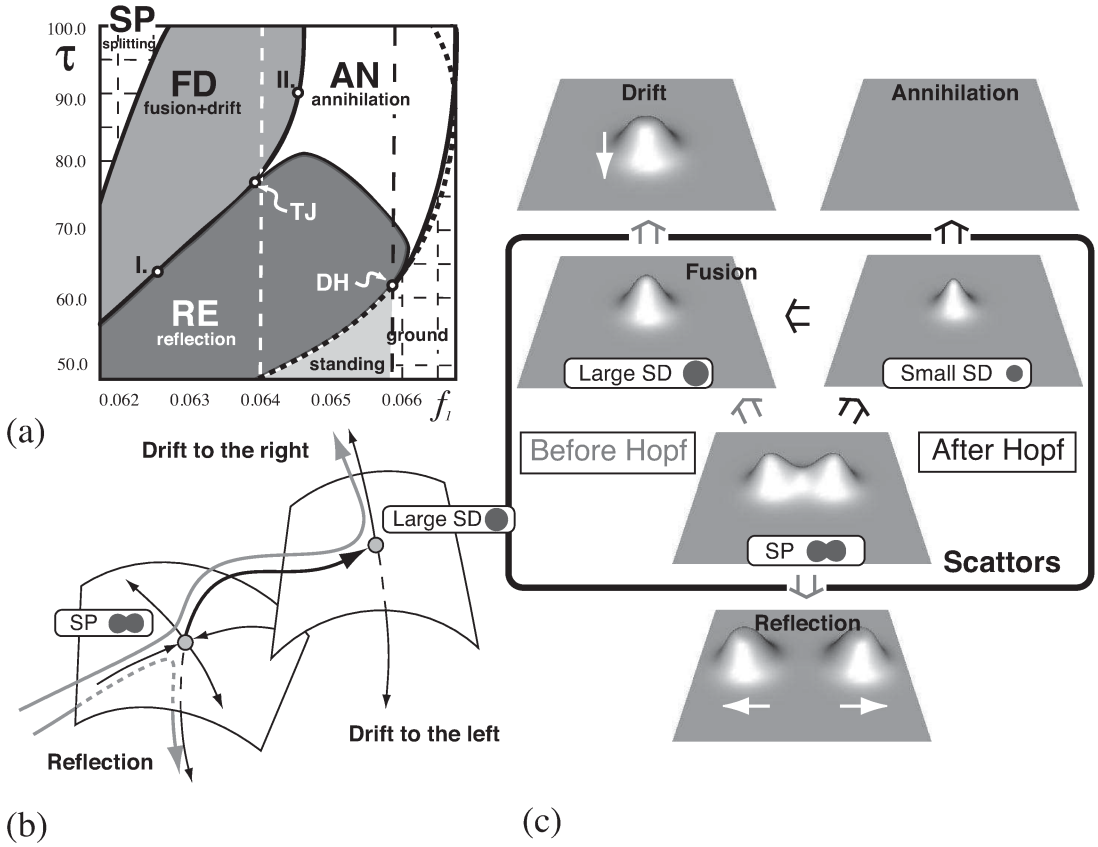


Figure 3. (a) Phase diagram for the outputs of head-on collisions with respect to $(f_1, \tau)$. There are three qualitatively different outputs, reflection (RE), fusion and drift (FD), and annihilation (AN). The black dashed and the white dotted lines indicate the Hopf and drift bifurcations for the standing disk (SD) spot, respectively. (b) A schematic diagram of scattors and their connections. Two saddle type of solutions standing peanut (SP) and large SD are connected by their unstable and stable manifolds. The fate of each orbit is determined by which side of the stable manifold of peanut contains its initial profile. The connecting manner reflects how large deformation occurs after collision. (c) Three scattors SP, large SD, and small SD and the change of connecting routes as parameters vary. When annihilation occurs, small SD plays a key role, which is connected to large SD via saddle-node bifurcation. Only $v$-component is shown here. For details, see the reference [22].

**3.3.1. FUSION-REFLECTION TRANSITION** We study how the behavior is switched from FD to RE around the transition point III $(f_1, \theta_i) \approx (0.064465, 14°)$. As $f_1$ is decreased, the output of the colliding spots is changed from RE to FD as shown in Figs.4(a)(b). Right after the collision, the spots travel for certain time with keeping

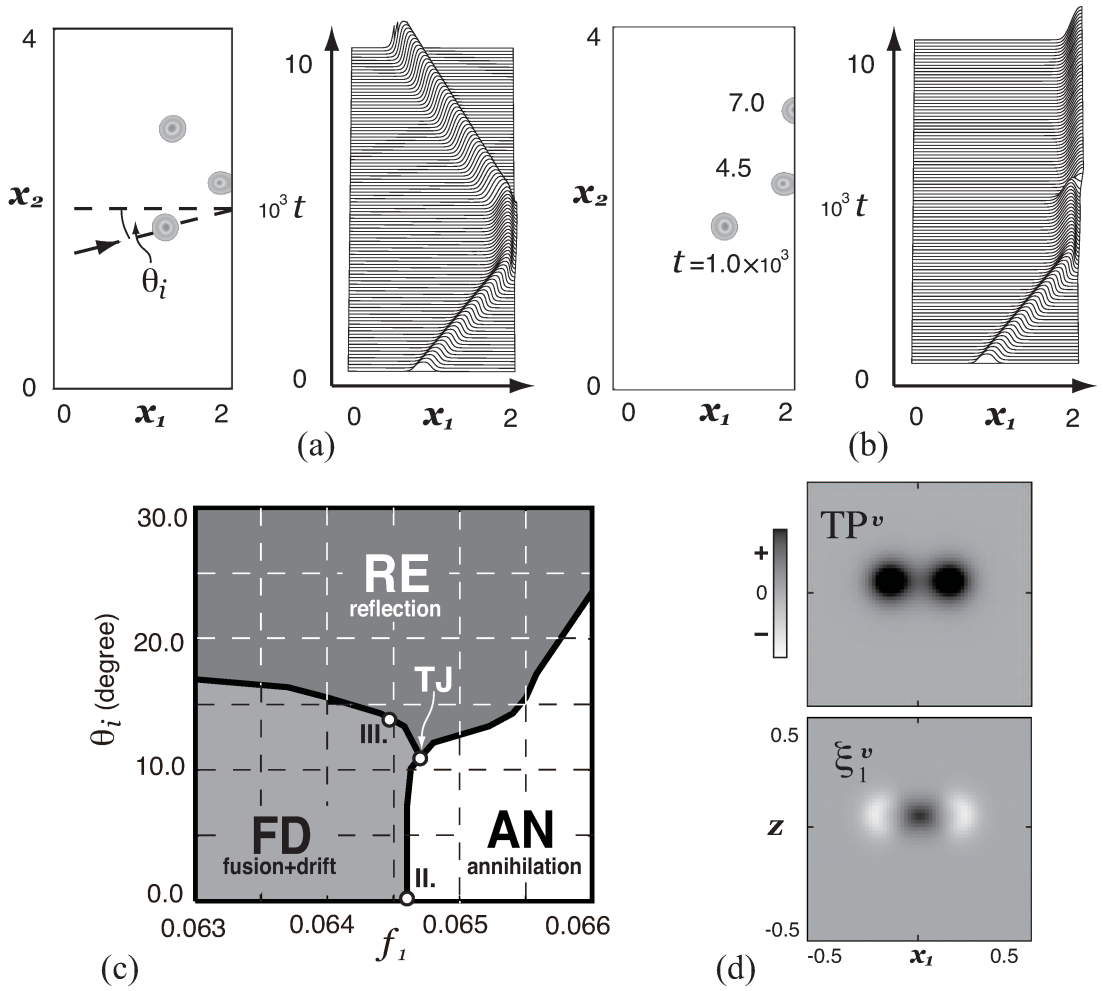


Figure 4. Spatio-temporal behaviors for oblique collision to the Neumann wall and the phase diagram of outputs in ($f_1$,$\theta_i$)-plane. (a) Traveling spot coming from the lower-left reflects to the upper-left after collision. We set to $(f_1, \tau) \approx (0.064465, 90)$ with the incident angle $\theta_i$ around 14°. As $f_1$ is decreased slightly, the transition from RE to FD occurs as shown in (b). In both cases there appear quasi-steady traveling peanuts (TPs) that persist for certain time before settling down to final states. (c) Phase diagram of output for oblique collision with respect to $(f_1, \theta_i)$. As the incident angle is increased, the reflection regime is expanded. (d) Profiles of TP scattor and the associated eigenmode $\xi_1$ with the largest eigenvalue of $\lambda \approx 0.015$ near the FD-RE phase boundary. The $\xi_1$ has two minima and one high maximum. Only $v$-component is shown here.

two peaks before they reflect each other or merge together. They look like a peanut shape. Such a transient peanut pattern can be captured as in Fig.4(d), namely getting on the moving coordinate $z = x_2 - ct$ with $c \approx 2.4 \times 10^{-4}$ of (2.1). The TP pattern is

unstable with the largest real eigenvalue ($\lambda_1 \approx 0.015$) and the associated eigenfunction $\xi_1$ is depicted as Fig.4(d). Its profile has two minima and one maximum, suggesting that merging or splitting occurs depending on the sign of the perturbation proportional to the eigenform. In fact it is confirmed numerically (see Fig.5 (a)) that the difference of sign induces that of output.

It is quite instructive and suggestive to see the interrelation among all relevant patterns to collision dynamics. Figure 5(b) shows solution branch of TS and TP families bifurcated from the drift points of SD patterns. The deformation from TP to TS is indicated by an up-pointing arrow in the middle part of TP branch in Fig.5(b). In view of Fig.5, the network structure of scattors (i.e., connecting manner among unstable patterns) changes as $f_1$ varies so that the passage of deformation also changes even if the manner of collision remains the same as before. Also note that scattors for the collision problem like TP play a key role to understand the deformation process of spots in heterogeneous media as will be discussed in the next section.

## § 4. DYNAMICS IN HETEROGENEOUS MEDIA

### § 4.1. REFRACTION AND REFLECTION AT JUMP HETEROGENEITY

Refraction and reflection are well-known phenomena in optics when light enters from air to water. We study similar problems for the traveling spot of (2.1) as if it were like a photon. We assume a heterogeneity of jump type along a line and study the behavior of traveling spot as the height of the jump and the incident angle vary. For definiteness, we introduce spatial heterogeneity to $f_1$ as $f_1(\boldsymbol{r}) = f_1^L + \epsilon\chi(\boldsymbol{r})$ where

$$\chi(\boldsymbol{r}) = \frac{1}{1+\mathrm{e}^{-\gamma x_1}}, \tag{4.1}$$

We set $f_1(-\infty, x_2) = f_1^L$ and $f_1(+\infty, x_2) = f_1^R$ with $\epsilon \equiv f_1^R - f_1^L$. The parameter $\gamma$ controls the steepness of the jump and is fixed to be 100. Note that the media varies in the $x_1$ direction only and $\epsilon$ controls the height of the jump. Moreover we take $\tau = 40.0$ in this section, which guarantees that the drift bifurcation becomes supercritical as in Fig.5(c) and the traveling velocity is increased when $f_1$ is decreased. For more detailed discussions, see the references of [37, 38].

Typical refraction and reflection are shown in Fig.1 as the height $\epsilon$ is varied. It is clear that spots can transmit the jump region when $\epsilon = 0$. Recalling that, for positive (resp. negative) $\epsilon$, the propagation velocity in the right half region is smaller (resp. larger) than that in the left half region due to the supercriticality of the drift bifurcation as in Fig.5(c), it is expected that the spot entering a higher velocity medium,

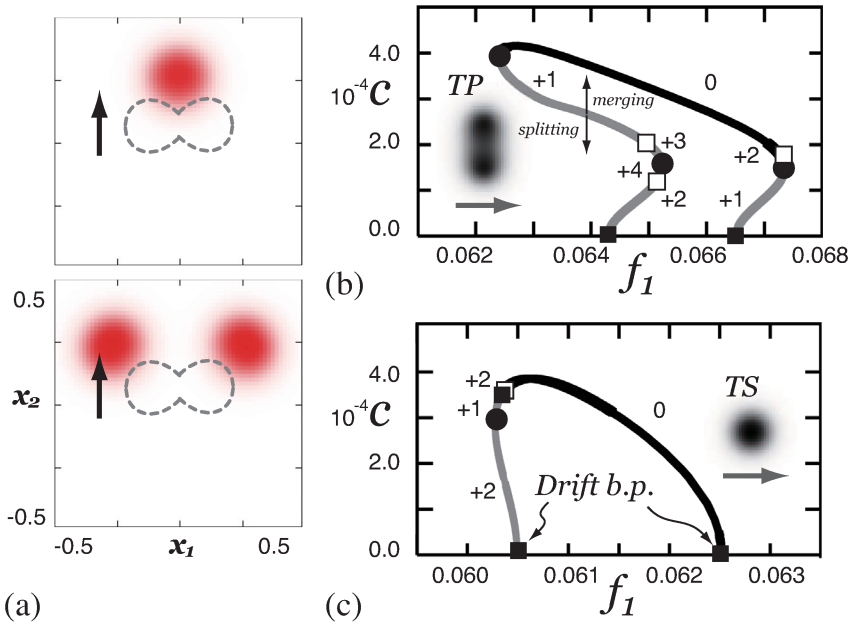


Figure 5. (a) The responses of the TP to the perturbations of the constant-multiples of the eigenfunction of Fig.4(d). If it is positive, then the middle part grows and it becomes a single TS like the upper figure. If it is negative, it splits into two TSs as in the lower figure. Only $v$-component is shown here. Spectral computations are done with the system size $1.5 \times 1.5$. (b) Global bifurcation diagram of traveling spot solutions to (2.1) for $\tau = 90$. The vertical axis corresponds to the propagation velocity of traveling spots. The solid and gray lines indicate the stable and unstable solutions. The black and white squares indicate the pitchfork (drift) and Hopf points and the black disks show the saddle node points, respectively. The number attached to each branch indicates that of unstable eigenvalues. TS emanates from SD via a drift bifurcation. TP solution is associated with the TS solution which loses its stability through the saddle-node bifurcation. (c) Global bifurcation diagram of spot solutions for $\tau = 40$. The right drift bifurcation from SD is supercritical and the emanated TS remains stable up to the Hopf instability. Crossing the saddle-node point, it deforms to a peanut-like shape, and it falls to the SP branch at the left drift bifurcation point.

i.e., $\epsilon \leq 0$ bends towards the perpendicular, and bends away from the perpendicular for $\epsilon \geq 0$. In fact, it is the case as is depicted in Fig.1(e), which shows the $\epsilon$-dependence of the refraction angle $\theta_t$. For negative $\epsilon$, the spot always transmits the jump line and no reflection occurs. On the other hand, for positive $\epsilon$, the transition from refraction to reflection occurs at some critical level $\epsilon_c$; the angle $\theta_t$ exceeds $\pi/2$. It is in a sense that the traveling spot turns back from a bad environment of lower velocity.

There are two issues to be discussed in the following.

1. What is the relation between the incident and refraction angles? Does the Snell's-like law hold for traveling spots ?

2. What is the separatrix for the transition from refraction to reflection ?

To answer these questions, we will derive a finite-dimensional system from our PDEs (2.1) near the drift bifurcation. Such a reduction is possible thanks to the fact that the traveling spots are spatially localized. A resulting system allows us to unveil a deeper mechanism behind these phenomena and capture the essential dynamics observed in the original PDEs.

It may be instructive to regard the refraction as a mapping from a traveling spot living in the homogeneous space located at $-\infty$ with the incident angle $\theta_i$ to that with the refraction angle $\theta_t$ living in the homogeneous space located at $+\infty$, and similarly for the reflection case. These mappings and the transition from refraction to reflection can be schematically depicted as in Fig.8(a).

## § 4.2. REDUCTION TO A FINITE DIMENSIONAL SYSTEM

The spot dynamics in two-dimensional system can be reduced to a finite-dimensional one when the associated parameter values are close to the drift bifurcation of $f_1 = f_1^c$ (see Fig.5(c)), namely the pulse velocity is slow.

Let us derive such a system in the following general setting with small parameter $\eta$ as $f_1 = f_1^c + \eta$,

$$\boldsymbol{u}_t = D\triangle\boldsymbol{u} + F(\boldsymbol{u}; f_1) \equiv \mathcal{L}(\boldsymbol{u}; f_1^c) + (\eta + \epsilon\chi(\boldsymbol{r}))\boldsymbol{g}(\boldsymbol{u}), \tag{4.2}$$

where $\boldsymbol{g}$ is a $N$-dimensional vector-valued function. Let $X := \{L^2(\mathbb{R}^2)\}^N$, $\boldsymbol{U}(t, \boldsymbol{r}) = (u_1, \cdots, u_N)^T \in X$ be an $N$-dimensional vector. We assume that the non-trivial standing pulse solution $S(\boldsymbol{r}; f_1)$ exists at $f_1 = f_1^c$, i.e., $\mathcal{L}(S; f_1^c) = 0$.

Let $L$ be the linearized operator as $L = \mathcal{L}(S(\boldsymbol{r}, f_1^c))'$. $L$ has a singularity at $f_1 = f_1^c$ consisting of drift bifurcation in addition to the translation-free 0 eigenvalues. That is, there exist two eigenfunctions $\boldsymbol{\phi}_i(\boldsymbol{r})$ and $\boldsymbol{\psi}_i(\boldsymbol{r})$ $(i = 1, 2)$ such that $L\boldsymbol{\phi}_i = 0$ and $L\boldsymbol{\psi}_i = -\boldsymbol{\phi}_i$, where $\boldsymbol{\phi}_i = \partial S/\partial x_i$. Note that $\boldsymbol{\phi}_i(\boldsymbol{r})$ and $\boldsymbol{\psi}_i(\boldsymbol{r})$ are odd functions. $\boldsymbol{\psi}_i(\boldsymbol{r})$ represents the deformation vector with Jordan form for the drift bifurcation.

Similar properties also hold for $L^*$. That is, there exist $\boldsymbol{\phi}_i^*$ and $\boldsymbol{\psi}_i^*$ such that $L^*\boldsymbol{\phi}_i^* = 0$ and $L^*\boldsymbol{\psi}_i^* = -\boldsymbol{\phi}_i^*$. Let $E = \mathrm{span}\{\boldsymbol{\phi}_i, \boldsymbol{\psi}_i\}$ and the eigenfunctions are normalized by $\langle\boldsymbol{\psi}_i, \boldsymbol{\phi}_j\rangle_{L^2} = \langle\boldsymbol{\psi}_i, \boldsymbol{\psi}_j^*\rangle_{L^2} = 0$, and,

$$\langle\boldsymbol{\phi}_i, \boldsymbol{\psi}_j^*\rangle_{L^2} = \langle\boldsymbol{\psi}_i, \boldsymbol{\phi}_j^*\rangle_{L^2} = \begin{cases} \pi & i = j, \\ 0 & i \neq j. \end{cases} \tag{4.3}$$

The motion of a spot $\boldsymbol{u}$ is essentially described by the two-dimensional vector functions of time $t$; $\boldsymbol{p} = (p_1, p_2)$ denotes the location of the spot; $\boldsymbol{q} = (q_1, q_2)$ denotes

its velocity. For small $\eta$, we can approximate a solution $\boldsymbol{u}$ by

$$\boldsymbol{U} = \tau(\boldsymbol{p})\left(S + \sum_{i=1}^{2} q_i \boldsymbol{\psi}_i + {q_1}^2\zeta_1 + {q_2}^2\zeta_2 + q_1q_2\zeta_3 + \eta\zeta_4\right), \tag{4.4}$$

where $\tau(\boldsymbol{p})$ is the translation operator with $(\tau(\boldsymbol{p})\boldsymbol{u})(\boldsymbol{r}) = \boldsymbol{u}(\boldsymbol{r} - \boldsymbol{p})$. The coefficient vectors of remaining quadratic terms $\zeta_k (k = 1, \cdots 4) \in E^{\perp}$ are defined by solutions of

$$\begin{cases} -L\zeta_1 = \dfrac{1}{2}F''(S){\boldsymbol{\psi}_1}^2 + \boldsymbol{\psi}_{1x_1}, \\ -L\zeta_2 = \dfrac{1}{2}F''(S){\boldsymbol{\psi}_2}^2 + \boldsymbol{\psi}_{2x_2}, \\ -L\zeta_3 = F''(S)\boldsymbol{\psi}_1\boldsymbol{\psi}_2 + \boldsymbol{\psi}_{1x_2} + \boldsymbol{\psi}_{2x_1}, \\ -L\zeta_4 = \boldsymbol{g}(S). \end{cases} \tag{4.5}$$

Substituting (4.4) into (4.2) and taking the inner product with the adjoint eigenfunctions, we obtain the principal part by the following system.

$$\begin{cases} \dot{\boldsymbol{p}} = \boldsymbol{q} - \epsilon\boldsymbol{\Gamma}^0(\boldsymbol{p}), \\ \dot{\boldsymbol{q}} = M_1|\boldsymbol{q}|^2\boldsymbol{q} + M_2\eta\boldsymbol{q} + \epsilon\boldsymbol{\Gamma}^1(\boldsymbol{p}). \end{cases} \tag{4.6}$$

The extra terms $\boldsymbol{\Gamma}^k (k = 0, 1)$ encode the heterogeneity as

$$\Gamma_i^0(\boldsymbol{p}) = \int_{\mathbb{R}^2} \chi(\boldsymbol{r})\boldsymbol{g}(S(\boldsymbol{r} - \boldsymbol{p})) \cdot \psi_i^*(\boldsymbol{r} - \boldsymbol{p})\mathrm{d}\boldsymbol{r},$$
$$\Gamma_i^1(\boldsymbol{p}) = \int_{\mathbb{R}^2} \chi(\boldsymbol{r})\boldsymbol{g}(S(\boldsymbol{r} - \boldsymbol{p})) \cdot \phi_i^*(\boldsymbol{r} - \boldsymbol{p})\mathrm{d}\boldsymbol{r}.$$

The effect of heterogeneity becomes acceleration (resp. deceleration) when $\epsilon\Gamma_i^1 >$ (resp. $<$) 0. Note that the heterogeneous term $\boldsymbol{\Gamma}^k(\boldsymbol{p})$ contains the information coming from the original PDE in terms of linearized eigenfunctions as well as the constants $M_1$ and $M_2$ in (4.6).

**Proposition 4.1.** *The constants $M_1$ and $M_2$ are given as follows:*

$$\begin{cases} \pi M_1 = \dfrac{1}{6}\langle F'''(S){\boldsymbol{\psi}_1}^3, \boldsymbol{\phi}_1^*\rangle_{L^2} + \langle F''(S)\boldsymbol{\psi}_1\zeta_1, \boldsymbol{\phi}_1^*\rangle_{L^2} + \langle \zeta_{1x_1}, \boldsymbol{\phi}_1^*\rangle_{L^2}, \\ \pi M_2 = \langle F''(S)\boldsymbol{\psi}_1\zeta_4, \boldsymbol{\phi}_1^*\rangle_{L^2} + \langle \boldsymbol{g}'(S)\boldsymbol{\psi}_1, \boldsymbol{\phi}_1^*\rangle_{L^2} + \langle \zeta_{4x_1}, \boldsymbol{\phi}_1^*\rangle_{L^2}. \end{cases} \tag{4.7}$$

The proof will be shown in the Appendix. Note that the last terms of the right-hand side, $\langle \zeta_{1x_1}, \boldsymbol{\phi}_1^*\rangle_{L^2}$ and $\langle \zeta_{4x_1}, \boldsymbol{\phi}_1^*\rangle_{L^2}$, are new and crucial ones added to the constants $M_1$ and $M_2$ in Theorem 2 of [6].

## § 4.3. OBLIQUE COLLISION AND OPTICS-LIKE LAW

Now we assume $\epsilon = |\eta|^{3/2}\hat{\epsilon}$, and introduce the following rescaling $\boldsymbol{q} = |\eta|^{1/2}\boldsymbol{Q}$ and $\tilde{t} = |\eta|^{1/2}t$. The leading order equations for (4.6) become

$$\begin{cases} \dot{\boldsymbol{p}} = \boldsymbol{Q}, \\ \dot{\boldsymbol{Q}} = |\eta|^{1/2}(M_1|Q|^2\boldsymbol{Q} + \mathrm{sgn}(\eta)M_2\boldsymbol{Q} + \hat{\epsilon}\boldsymbol{\Gamma}^1(\boldsymbol{p})), \end{cases} \tag{4.8}$$

where we omit the tilde for simplicity. Here negative signs of coefficients are numerically confirmed as $M_1 \approx -61.349 < 0$ and $M_2 \approx -0.264 < 0$ from Proposition 4.1. The heterogeneous term of the first equation disappears thanks to the above scaling near the pitchfork bifurcation. For the homogeneous case $\hat{\epsilon} = 0$, the second equation of (4.8) can be rewritten as $\dot{\boldsymbol{Q}} = -|\eta|^{1/2}\nabla_{\boldsymbol{Q}}W$, where $W(\boldsymbol{Q}) = -M_1|\boldsymbol{Q}|^4/4 - \mathrm{sgn}(\eta)M_2|\boldsymbol{Q}|^2/2$. The velocity of traveling spot for this case is given by the invariant circle of $W$, i.e., $|\boldsymbol{Q}|^2 = Q_1^2 + Q_2^2 = -\mathrm{sgn}(\eta)M_2/M_1 \equiv Q_0^2$ for $\eta < 0$. Since $W(\boldsymbol{Q})$ is a function of $Q = |\boldsymbol{Q}|$, we can rewrite it as $W(Q)$ such that $W(Q_0) = \min W(Q) = -M_2^2/4M_1$. Hereafter we only consider the case of $\eta < 0$.

From the symmetry of (4.1), the component of the heterogeneous term $\boldsymbol{\Gamma}^k(\boldsymbol{p})$ which is tangent to the heterogeneity becomes zero, i.e., $\boldsymbol{\Gamma}^k(\boldsymbol{p}) = (\Gamma_1^k(\boldsymbol{p}), 0)^T$. As shown in Fig.6, the heterogeneous term $\Gamma_1^1(\boldsymbol{p})$ (resp. $\Gamma_1^0(\boldsymbol{p})$) is a negative (resp. positive) even function which decays exponentially to 0 as $p_1 \to \pm\infty$, and it has the minimum (resp. maximum) at $p_1 = 0$. They keep the same profiles in the direction parallel to the $p_2$ axis. It is easy to see that there exist no equilibria of (4.8) with $|\boldsymbol{Q}| = 0$ except which located at $p_1 = \pm\infty$. It should be remarked that the second component of the velocity $Q_2$ is conserved during crossing the jump line if we neglect the higher order terms $O(|\eta|)$ owing to the fact that the second component of the heterogeneous term is equal to zero.

**4.3.1. LAW OF REFRACTION** Let us consider the relation between angles of incidence and output. Since the angle near the jump line is not well-defined, we resort to the asymptotic behaviors of spots far from the jump line with the aid of $\lim_{p_1 \to \pm\infty} \Gamma_1^k(\boldsymbol{p}) = 0$. Let $\boldsymbol{Q}(0)$ be the initial velocity which is given at the initial position $\boldsymbol{p}(0)$ located sufficiently away from jump line and $\boldsymbol{Q}(\infty)$ be the asymptotic velocity after refraction or reflection. Then we define the angle of incidence $\theta_i$ and the angle of output $\theta_o$ by

$$\theta_i = \arctan\left(\frac{Q_2(0)}{Q_1(0)}\right),\ \theta_o = \arctan\left(\frac{Q_2(\infty)}{Q_1(\infty)}\right), \tag{4.9}$$

where $\boldsymbol{Q}(0) = Q_0\boldsymbol{e}(\theta_i)$ with $\boldsymbol{e}(\theta) = (\cos\theta, \sin\theta)^T$.

The issue is to study the fate of the orbit starting from $p_1 = -\infty$ for a given jump heterogeneity of (4.1). When it goes to $p_1 = +\infty$(resp. $-\infty$) as $t \to +\infty$, it means

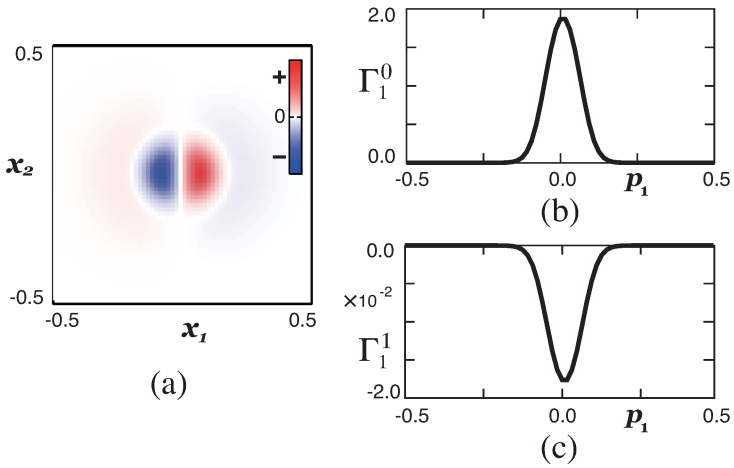


Figure 6. (a) The $v$-component profile of the deformation vector $\psi_1$ of standing disk spot solution. The left (right)-half part has negative (positive) sign. The profiles along $p_1$-axis of the heterogeneous terms $\Gamma_1^0(\boldsymbol{p})$ and $\Gamma_1^1(\boldsymbol{p})$ are shown in (b) and (c).

that the spot transmits (resp. reflects from) the jump line. Depending on the height $\hat{\epsilon}$, the orbits behave as in Figs.7(a)(b). The output $\theta_o$ belongs to one of the followings: transmission $\theta_t = \theta_o$ for $0 < \theta_o < \pi/2$, and reflection $\theta_r = \pi - \theta_o$ for $\pi/2 < \theta_o < \pi$.

Now we consider the transmission case in which refraction is observed. Recalling that the heterogeneous term decays monotonically as $\lim_{|p_1|\to\infty} \Gamma_1^k(\boldsymbol{p}) = 0$, the velocity change occurs mainly around the jump line. In view of Fig.7(d), the transmission angle $\theta_t$ is determined by the incident angle $\theta_i$ via sine functions, namely the ratio $\sin\theta_i / \sin\theta_t$ is constant for each fixed $\hat{\epsilon}$. This reminds us the Snell's law in optics, in fact a Snell's-like holds but its dependency on the velocities is reversed as will be explained shortly.

Now recall that the drift bifurcation is supercritical for $\tau = 40$, then the propagation velocities are calculated from (4.6) as $\sqrt{M_2/M_1}$ in the left half-plane and $\sqrt{(1-\hat{\epsilon}|\eta|^{1/2})M_2/M_1}$ in the right half-plane. Hence the relative velocity of the two media is defined by $n = \sqrt{1-\hat{\epsilon}|\eta|^{1/2}}$. As we remarked at the end of the last section, the tangential component of $\boldsymbol{Q}$ is conserved in the rescaled system. Expressing the tangential velocity by sine functions, this is equivalent to the following relation.

$$\frac{\sin\theta_i}{\sin\theta_t} = n. \tag{4.10}$$

The well-known Snell's law in optics states that the ratio of the sines of the angles of incidence and refraction is equivalent to the ratio of phase velocities in the two media. Here the the ratio is equal to the opposite ratio of two velocities of traveling spots. The numerical results in Figs.7(c)(d) agree with the relation (4.10).

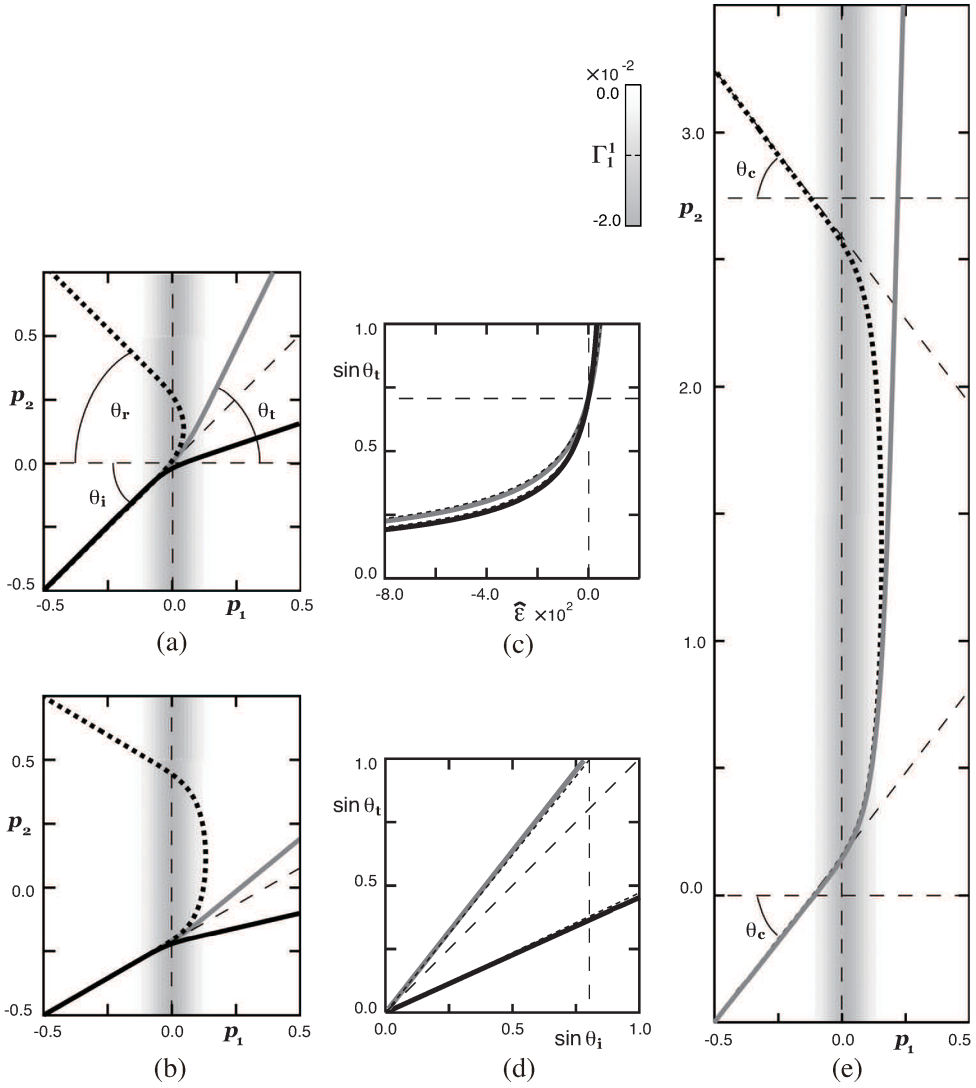


Figure 7. Orbit flows in the $(p_1, p_2)$ plane for (a) $\theta_i = \pi/4$ and (b) $\pi/6$. The parameter $\eta$ is set to $-1.0 \times 10^{-4}$. The solid, gray, and dotted lines show for $\hat{\epsilon} = -350$, 35, and 70, respectively. The heterogeneous term $\Gamma_1^1(\boldsymbol{p})$ is indicated by the background gray gradation. The $\hat{\epsilon}$-dependence of the transmission angle $\theta_t$ for ODE dynamics are shown in (c). The horizontal broken line indicates $\theta_t = \theta_i$. (d) The incident angle $\theta_i$-dependence of $\theta_t$. The solid and gray lines show $\hat{\epsilon} = -350$ and 35. The vertical broken line indicates the critical angle $\theta_c$ for $\hat{\epsilon} = 35.0 > 0$. The graphs obtained from (4.10) are depicted by the dotted lines in (c) and (d). (e) Orbit flows are depicted for the transition from transmission to reflection around $\theta_i \approx \theta_c$ for $(\hat{\epsilon}, \eta) = (35, -1.0 \times 10^{-4})$.

**4.3.2. TRANSITION FROM TRANSMISSION TO REFLECTION** In this subsection, we focus on the transition from transmission (TR) to reflection (RE) as the height $\hat{\epsilon}$ or the incident angle $\theta_i$ is increased. For positive $\hat{\epsilon} > 0$, $\theta_t$ becomes larger

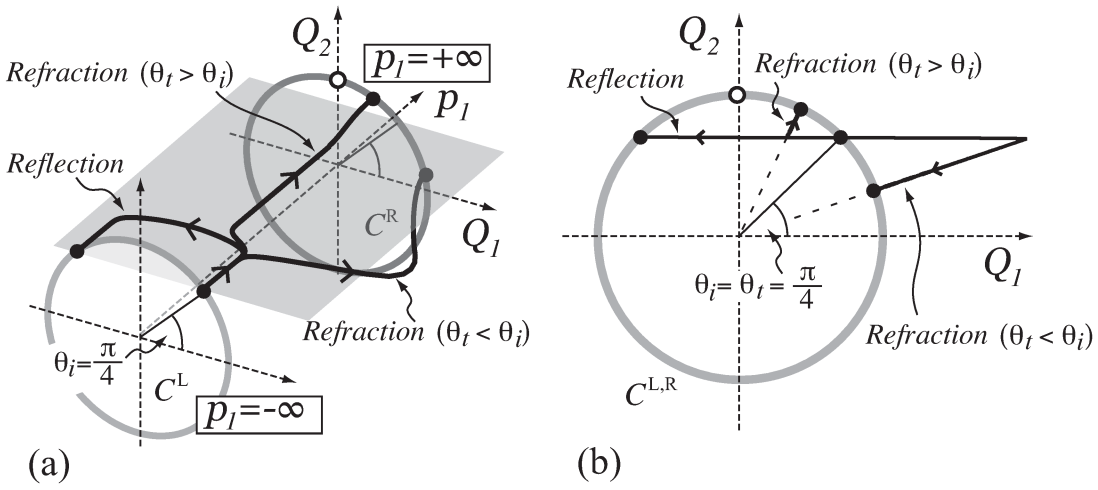


Figure 8. (a) Schematic picture of orbit flows in three-dimensions of $(p_1, Q_1, Q_2)$. The solid circles $C^{\mathrm{L,R}}$ show the invariant circles of TS solutions at $p_1 = \mp\infty$, respectively. The solid curves indicate the orbit flows starting from $\theta_i = \pi/4$ for the reflection of $\hat{\epsilon} = 70$ and refraction for 35 and $-350$, respectively. The white disk on $C^{\mathrm{R}}$ indicates the traveling spot solution moving parallel to the jump line, corresponding to $\theta_t = \pi/2$. It plays a role of scattor for the transition between reflection and refraction behaviors. (b) The projection of orbit flows onto the $(Q_1, Q_2)$-plane. The refraction behaviors initially move on the plane where $Q_2$ is conserved, indicated by the gray plane in (a), and then they gradually depart from that into the final destination of TS on $C^{\mathrm{R}}$ along its stable manifold in the direction of $\boldsymbol{e}(\theta_t)$.

than $\theta_i$ as shown in Fig.7(d). The orbit of transmitted spot gradually approaches the line parallel to the jump line, as $\theta_i$ is increased. Eventually, $\theta_t$ reaches $\pi/2$ at some critical incident angle $\theta_i = \theta_c$. The larger $\hat{\epsilon}$ (i.e., the smaller $n$) is, the smaller $\theta_c$ is. For $\theta_i$ greater than $\theta_c$, the spot turns back to the left-half plane. A careful numerical simulation shows as in Fig.7(e) that the orbit just before or after the transition point from TR to RE behaviors behaves like a quasi-traveling spot moving almost parallel to the jump line for a certain time, then it transmits or reflects depending on the parameter. There is a tendency that the distance between the jump line and this quasi-traveling spot becomes larger, as $\theta_i$ becomes closer to $\theta_c$. It is expected that this quasi-orbit eventually converges to **the traveling spot moving parallel to the jump line in the homogeneous space located at** $p_1 = \infty$. The PDE counterpart is also numerically obtained. This type of separating orbit is called a scattor living in the homogeneous space located at $\pm\infty$. When $\lim_{|p_1|\to\infty} \Gamma_1^k(\boldsymbol{p}) = 0$, the system recovers the rotational and translational invariance, i.e., the spots go straight in the homogeneous

space. There exist the invariant circles $C^{L,R}$ of $Q_1(t)^2 + Q_2(t)^2 = Q_0^2$ in the $(Q_1, Q_2)$-plane at left and right infinity.

Here we introduce the complex variables $z = Q_1 + iQ_2$, and we can rewrite as

$$\dot{z} = |\eta|^{1/2}(M_1|z|^2 z - M_2 z + \hat{\epsilon}\Gamma_1^1). \tag{4.11}$$

Moreover, letting $z = Qe^{i\theta}$, we rewrite (4.11) as

$$\begin{cases} \dot{Q} = |\eta|^{1/2}(M_1 Q^3 - M_2 Q + \hat{\epsilon}\Gamma_1^1 \cos\theta), \\ \dot{\theta} = -|\eta|^{1/2}\hat{\epsilon}\dfrac{\Gamma_1^1}{Q}\sin\theta. \end{cases} \tag{4.12}$$

It is easily seen that $\dot{\theta} < 0$ (resp. $\dot{\theta} > 0$) for $\hat{\epsilon} < 0$ (resp. $\hat{\epsilon} > 0$) and $\dot{\theta}$ gets closer to zero after sufficiently long time when spot moves far apart from a jump line. Actually, it is found by the stability analysis of (4.12) that the traveling spot solution on $C^{\mathrm{L,R}}$ has one zero and one negative eigenvalue of $2|\eta|^{1/2}M_2$. The zero eigenvalue is associated with the neutral deformation vector perpendicular to the moving direction $\boldsymbol{e}(\theta)$. We expect that the orbit flow slowly approaches to the TS solution on $C^{\mathrm{R}}$ along its stable manifold in the moving direction $\boldsymbol{e}(\theta_t)$. In particular, the fates of orbit near the transition from transmission to reflection are sorted out according to which side of the stable manifold of TS ($\theta_t = \pi/2$) the orbit belongs. Once $\theta_t$ exceeds $\pi/2$, the orbit turns back to the jump line and accelerate to the left by the heterogeneity of $\epsilon\Gamma_1^1(\boldsymbol{p})$. The details will be shown in [38]. In the next section, we will discuss similar types of scattors.

## § 5. SPLITTING AND TRAVELING PEANUT SCATTOR LOCATED AT INFINITY

Heterogeneities also trigger the splitting instability besides refraction and reflection as discussed in previous sections. It is known for spontaneous splitting, i.e., without external effects such as heterogeneities, that a saddle-node bifurcation is responsible for such a splitting as was discussed in [26, 27]. On the other hand our basic setting is that the traveling disk spots (TSs) on both sides of line heterogeneity are locally stable and hence they do not split spontaneously in each homogeneous space. Nevertheless splitting can occur when the traveling spot crosses the line heterogeneity. A natural question is **what is the underlying mechanism that is responsible for the splitting in heterogeneous media ?** It turns out that traveling peanut (TP) patterns as shown in Fig.5 play a key role to answer it. Loosely speaking, the traveling spot is distorted when it encounters the heterogeneity, and if the associated deformation is strong enough to escape from the basin of TS, then it starts to split. TP is located on the basin boundary and its stable manifold is a separator between splitting and non-splitting depending on

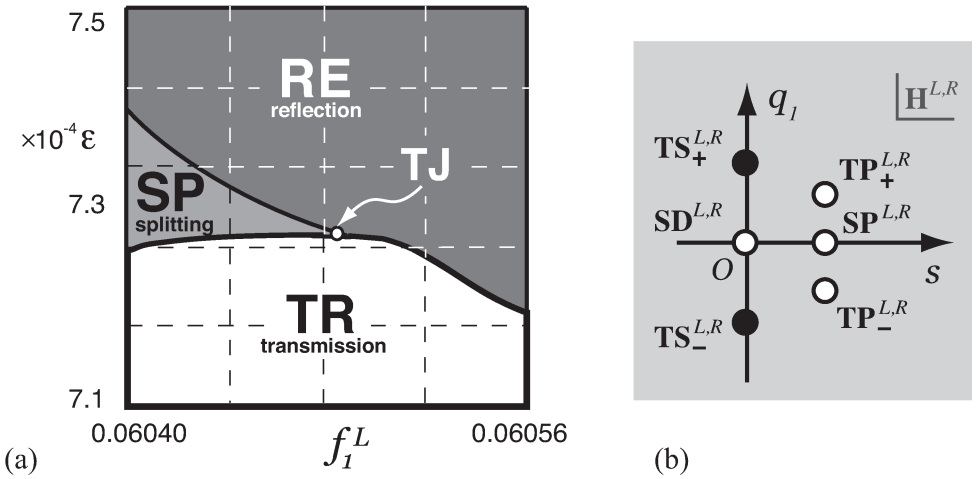


Figure 9. (a) Phase diagram for the outputs of traveling spots with heterogeneity with respect to $(f_1^L, \epsilon)$. Note that the parameter $f_1^L$ are chosen in the neighborhood of the saddle-node point of TS branch in Fig.5(c). There are three qualitatively different outputs, reflection (RE), transmission (TR), and splitting (SP). (b) Schematic picture of spot solutions in homogeneous spaces $\mathrm{H}^{\mathrm{L,R}}$ projected onto $(q_1, s)$-plane. The superscripts L,R depends on whether the homogeneous space locates at left or right infinity of $p_1$. The subscripts $\pm$ show the propagating directions of traveling objects corresponding to the sign of $q_1$. The axis $s$ indicates the amplitude of deformation into splitting.

the parameters. The size of the basin of TS shrinks as the distance to a saddle-node point becomes shorter, for instance, $f_1$ approaches 0.0604 (the location of the saddle-node point) as in Fig.5(c) for $\tau = 40$. See Fig.1 of [37] for more precise descriptions of TS and TP branches. Therefore even for the tiny jump, the spot can easily split when the parameter is close to the saddle-node point. In what follows we only consider the case in which the spot meets the jump line at right angle ($\theta_i = 0$). The phase diagram of Fig.9(a) shows how the outputs depend on the parameter $(f_1^L, \epsilon)$ where $\epsilon$ is the height of the jump. As is expected, the splitting behaviors are observed when the parameter $f_1^L$ is close to the saddle-node point of TS solutions. What we observe here are transmission (TR), splitting (SP), and reflection (RE). As $f_1^L$ is increased and becomes greater than the triple junction (TJ) point of $f_1^L \approx 0.06047$, the SP regime disappears and only TR and RE are observed.

The splitting behavior is quite interesting, in fact, for $(f_1^L, \epsilon) \approx (0.06046, 7.2817 \times 10^{-4})$, the orbit first crosses the jump line, then turns back and crosses the line again, finally it splits into two traveling spots as in Fig.10(b). In order to understand this behavior as well as transitions among TR, SP, and RE, it is necessary to introduce the two homogeneous spaces $\mathrm{H}^{\mathrm{L,R}}$ located at $p_1 = \pm\infty$ (see Fig.9(b)), namely $f_1 \equiv f_1^L$ in

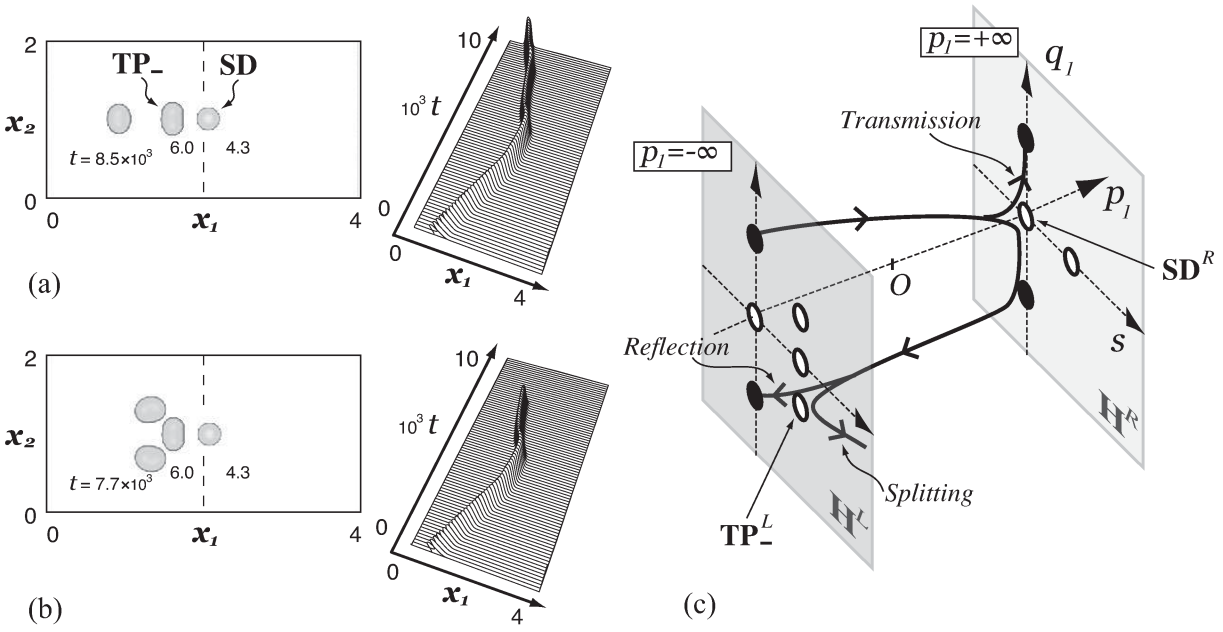


Figure 10. (a) Response of the traveling spot coming from the left when it meets the heterogeneity. We set to $(f_1^L, \epsilon) \approx (0.06046, 7.2817 \times 10^{-4})$. The left two figures show the behaviors when the spots turn back and cross the jump line for the second time. The left upper figure first shows the initiation of splitting, but it recovers the original shape afterwards. As $\epsilon$ is decreased slightly, the transition from reflection to splitting occurs as shown in the left lower figure (b). The middle figures show the associated time evolutions of the cross section at $x_2 = 1$ along the $x_1$-axis. In both cases there appear quasi-steady traveling peanuts (TPs) that persist for a certain time before settling down to each final state. (c) Schematic picture of orbit flows in the three-dimensions of $(p_1, q_1, s)$ near triple junction point of Fig.9(a). The orbits starting from $\mathrm{TS}_+^{\mathrm{L}}$ are sorted out along the heteroclinic connection between $\mathrm{SD}^{\mathrm{R}}$ and $\mathrm{TP}_-^{\mathrm{L}}$.

$\mathrm{H}^{\mathrm{L}}$ and similarly for $\mathrm{H}^{\mathrm{R}}$. This is because the separatrix responsible for these transitions are the orbits connecting the solutions living in those homogeneous spaces as illustrated in Fig.10(c). The solutions in $\mathrm{H}^{\mathrm{L,R}}$ have super and sub scripts like $\mathrm{TS}_+^{\mathrm{L}}$: the superscript denotes to which homogeneous space the solution belongs and the subscript shows the traveling direction. See the caption of Fig.9 for details.

It is clear that the TR behavior corresponds to the orbit starting from $\mathrm{TS}_+^{\mathrm{L}}$ and ending up with $\mathrm{TS}_+^{\mathrm{R}}$. In view of the phase diagram of Fig.9(a), the transition from TR to RE occurs for larger values of $f_1^L$ as the height $\epsilon$ is increased. On the other hand, for smaller values of $f_1^L$, we observe the transitions as $\epsilon$ is increased: TR $\to$ SP $\to$ RE as mentioned above. Although it may sound paradoxical, in order to understand

these transitions simultaneously, we look at the most degenerate situation in the phase diagram of Fig.9(a), i.e., the TJ point. There is a degenerate network of heteroclinic orbits consisting of connecting orbits between two homogeneous spaces $\mathrm{H}^{\mathrm{L,R}}$. Those connecting orbits are $\mathrm{TS}^{\mathrm{L}}_{+} \to \mathrm{SD}^{\mathrm{R}}$, $\mathrm{SD}^{\mathrm{R}} \to \mathrm{TS}^{\mathrm{R}}_{+}$, $\mathrm{SD}^{\mathrm{R}} \to \mathrm{TS}^{\mathrm{R}}_{-}$, $\mathrm{TS}^{\mathrm{R}}_{-} \to \mathrm{TP}^{\mathrm{L}}_{-}$, $\mathrm{TP}^{\mathrm{L}}_{-} \to \mathrm{TS}^{\mathrm{L}}_{-}$, and $\mathrm{TP}^{\mathrm{L}}_{-} \to$ two different $\mathrm{TS}^{\mathrm{L}}_{-}$. At the TJ point, the orbit starting from $TS^{+}_{L}$ is on this degenerate network. A tiny perturbation in the parameter space $(f^{L}_{1}, \epsilon)$ induces an unfolding of the degenerate network and either TR, SP or RE emerges depending on the direction of the perturbation as is shown in Fig.10(c). The degenerate network of heteroclinic connections among scattors is deserved to be called an **organizing center** for the outputs of traveling spots for the jump heterogeneity. The results in this section are based on the numerical path-tracking of global branches of relevant patterns as well as careful numerical simulations of (2.1). As a future work, it is a challenge to show rigorously such a network connection, in particular, the organizing center with the aid of reduction method discussed in Section 4.

## § 6. CONCLUDING REMARKS

We have studied refraction, reflection, and splitting phenomena for the system (2.1) and a special class of solutions called the scattor plays a crucial role to understand the transition dynamics among them. In the following remarks, we take a slightly different type of three-component reaction diffusion system and discuss similar problems in the previous sections. It turns out that exactly the same type of scattors appear as before, but at the same time, there is a difference depending on how the heterogeneity is introduced in the system. The system reads

$$\begin{cases} u_t = D_u \nabla^2 u + f(u) - k_3 v - k_4 w + k_1, \\ \tau v_t = D_v \nabla^2 v + u - v, \\ \theta w_t = D_w \nabla^2 w + u - w, \end{cases} \tag{6.1}$$

where $f(u) = u - u^3$, $k_1$, $k_3$, $k_4$ are positive parameters, and $D_u, D_v, D_w > 0$ are diffusion coefficients. This model was originally proposed as a qualitative model describing gas-discharge phenomena [2, 31]. Without the second inhibitor, i.e., $w \equiv 0$, this is reduced to the well-known FitzHugh-Nagumo equations so that (6.1) can be regarded as a generalized FitzHugh-Nagumo system via adding an another inhibitor $w$. Here we employ the following parameters: $(D_u, D_v, D_w) = (0.9 \times 10^{-4}, 1.0 \times 10^{-3}, 1.0 \times 10^{-2})$, $(k_2, k_3, k_4) = (2.0, 1.0, 8.5)$ for kinetic parameters and $(\tau, \theta) = (40, 1)$ for time constants. The parameter $k_1$ is a control parameter and we introduce the jump heterogeneity along the line in this parameter [24].

## § 6.1. TRAVELING PEANUT SCATTOR FOR A GENERALIZED FITZHUGH-NAGUMO SYSTEM

Figure 11 shows a behavior of traveling spot encountering a line heterogeneity of jump type at right angle for the model system (6.1). As the height of the jump is decreased, the spot changes its behavior from splitting of Fig.11(a) to transmission of (b). Numerics also shows an interesting transient pattern, namely a traveling peanut (TP); just before the splitting, it travels for a while with keeping the peanut shape, similarly the same TP pattern appears before merging into one TS for the transmission case. Such a TP pattern can be detected and has only one real positive eigenvalue whose associated eigenfunction has a sharp peak similar to Fig.4(d) indicating that its positive (resp. negative) perturbation is responsible for merging (resp. splitting). Such an unstable pattern persists for a long time as the height of the jump approaches the critical level. Therefore, at exactly the separation point between splitting and transmission, it survives for infinite time and converges to the unstable TP pattern living in the homogeneous space with $k_1 \equiv k_1^R$ located at right infinity. This suggests that the traveling peanut spot living in the homogeneous space at right infinity is a scattor (i.e., saddle point) separating two regimes, which supports the view point discussed in Section 5.

## § 6.2. HETEROGENEITY-INDUCED ORDERED PATTERNS (HIOPs) AND PATTERN GENERATOR

The heterogeneity in $f_1$ of (2.1) does not affect the existence of the constant background state $\boldsymbol{u}_0 = (1, 0, 0)$, since it is introduced in multiplicative way. This is not the case for (6.1), if we introduce the heterogeneity in $k_1$ in an additive way, i.e., such constant background state $\boldsymbol{u}_0$ is no more a solution to (6.1). Since the critical states associated with $k_1^{\mathrm{L}}$ and $k_1^{\mathrm{R}}$ are different, a class of new solutions instead emerges, which connects the left rest state to the right one to compensate the jump. It turns out that there are many such heteroclinic orbits including both stable and unstable ones depending on the parameters. This means that there are options for the background state in the case of (6.1). We call those solutions the heterogeneity-induced-ordered-patterns (HIOPs), which have been found and classified in [24, 25, 36, 43] for the case of jump and bump types in 1D and 2D cases. The traveling pulse or spot displays a variety of dynamics when it collides HIOPs at the jump point such as transmission, pinning, splitting, annihilation and so on. Those HIOPs are interrelated each other as appropriate parameters are varied and various types of instabilities and singularities are detected in the global bifurcation diagram, which actually allows us to understand the dynamics in heterogeneous media. For instance, the pinning and de-pinning phenomena of the trapped pulse around the heterogeneity of bump type as discussed in [36]. The trapped pulse oscillates back and forth inside of bump and can be released as the height is

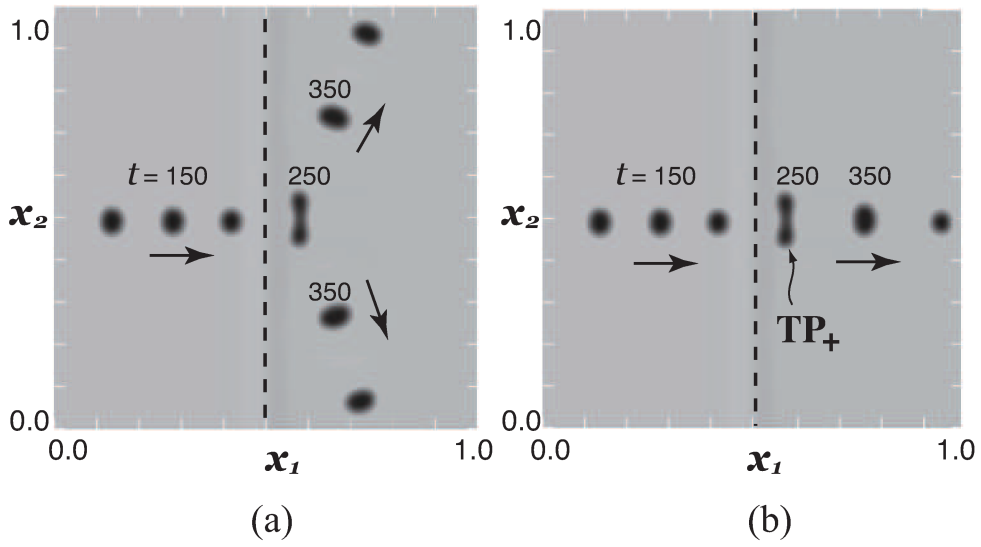


Figure 11. Traveling peanut scattor for the generalized FitzHugh-Nagumo system (6.1). (a) Time evolution sequence of a traveling spot coming from the left in heterogeneous media with $(k_1^L, k_1^R) \approx (-7.1, -6.754)$. The jump line of the heterogeneity is indicated by the broken line. A traveling spot ($t = 150$) becomes a traveling peanut ($t = 250$) just after colliding with the HIOP, the unstable traveling peanut then splits into two traveling spots ($t = 350$). (b) As $k_1^R$ is slightly decreased to $-6.755$, a traveling peanut right after collision at ($t = 250$) merges into a stable traveling spot ($t = 350$). For details, see the reference [24].

decreased, i.e., de-pinning. This can be explained by the fact that periodic motion of pulse approaches homoclinic or heteroclinc orbits depending on the shape of the bump after reducing the PDE dynamics to the associated ODE dynamics [36].

Finally, we describe about the class of spontaneous pattern generation (SPG), which is also one of the exciting dynamics as if it were alive. One of the well-known examples is the self-replicating pattern (or wave-splitting) first discovered in experiments [4, 9], then numerically [29], and some analysis have been done, for instance, [17, 26]. There are many other examples of SPG such as [10], for instance, however here we focus on the SPG created by heterogeneities as indicated by [30, 43]. It is quite remarkable that the simplest heterogeneity of jump type can produce such dynamics as shown numerically in [43]. To find a mechanism behind the scene, it may be helpful to recall the pinning-depinning dynamics studied in [36]. Namely a traveling pulse is trapped by a heterogeneity of bump type and it oscillates back and forth within the bump, but it can be released as the height of the bump is decreased. This can be regarded as a one pulse generator but it needs an external control of the height of bump, therefore it does not

deserve to be called a SPG. What is needed here is that newly born oscillating pulse should be created spontaneously near the heterogeneity even after the first pulse is emitted to the outside of the heterogeneity. In other words there must be a seamless cycle of creation and emitting pulses without external force. Very recently one characterization for the onset of pulse generation caused by a jump heterogeneity is proposed for (6.1) in [23] by studying the global interrelations of all relevant solutions to SPG. It can be regarded as a conversion mechanism from time-periodic pulse motion localized near the jump point to releasing it to outside of the heterogeneity. More detailed discussion will be reported elsewhere.

## ACKNOWLEDGEMENTS

The topics described in this paper are based on the collaborations and discussions with K. Nishi, A. Sekisaka, K. Suzuki, K. Tanaka, K.-I. Ueda, M. Yadome, and X. Yuan. Y. N. is deeply indebted to the organizing committee for "Far-from-equilibrium-dynamics" conference in Kyoto 2011 (FFED2011) who allowed me to write this paper. This work was partially supported by the Grant-in-Aid for Scientific Research under Grant No. B21340019 and 21120003 and for Young Scientists under Grant No.B20740224.

## § 7. APPENDIX

### § 7.1. Proof of Proposition 2.1 (Constants of $M_1$ and $M_2$ )

The derivations of (4.6) and (4.7) are given in this appendix. The correction terms to the results shown in [6] are obtained. We consider the inner products with $\boldsymbol{\phi}_1^*$ and $\boldsymbol{\phi}_2^*$,

$$
\begin{cases}
\langle \boldsymbol{U}_t, \boldsymbol{\phi}_1^* \rangle_{L^2} = \dot{q}_1 \langle \boldsymbol{\psi}_1, \boldsymbol{\phi}_1^* \rangle_{L^2} - \dot{p}_1 q_1^2 \langle \zeta_{1x_1}, \boldsymbol{\phi}_1^* \rangle_{L^2} \\
-\dot{p}_1 q_2^2 \langle \zeta_{2x_1}, \boldsymbol{\phi}_1^* \rangle_{L^2} - \dot{p}_2 q_1 q_2 \langle \zeta_{3x_2}, \boldsymbol{\phi}_1^* \rangle_{L^2} - \dot{p}_1 \eta \langle \zeta_{4x_1}, \boldsymbol{\phi}_1^* \rangle_{L^2}, \\
\langle \mathcal{L}(\boldsymbol{U}), \boldsymbol{\phi}_1^* \rangle_{L^2} = \left( \frac{1}{6} \langle F'''(S) \boldsymbol{\psi}_1{}^3, \boldsymbol{\phi}_1^* \rangle_{L^2} + \langle F''(S) \boldsymbol{\psi}_1 \zeta_1, \boldsymbol{\phi}_1^* \rangle_{L^2} \right) q_1^3 \\
+ \left( \frac{1}{2} \langle F'''(S) \boldsymbol{\psi}_1 \boldsymbol{\psi}_2{}^2, \boldsymbol{\phi}_1^* \rangle_{L^2} + \langle F''(S) \boldsymbol{\psi}_1 \zeta_2, \boldsymbol{\phi}_1^* \rangle_{L^2} + \langle F''(S) \boldsymbol{\psi}_2 \zeta_3, \boldsymbol{\phi}_1^* \rangle_{L^2} \right) q_2^2 q_1 \\
+ \eta \left( \langle F''(S) \boldsymbol{\psi}_1 \zeta_4, \boldsymbol{\phi}_1^* \rangle_{L^2} + \langle \boldsymbol{g}'(S) \boldsymbol{\psi}_1, \boldsymbol{\phi}_1^* \rangle_{L^2} \right) q_1,
\end{cases} \tag{7.1}
$$

$$
\begin{cases}
\langle \boldsymbol{U}_t, \boldsymbol{\phi}_2^* \rangle_{L^2} = \dot{q}_2 \langle \boldsymbol{\psi}_2, \boldsymbol{\phi}_2^* \rangle_{L^2} - \dot{p}_2 q_2^2 \langle \zeta_{2x_2}, \boldsymbol{\phi}_2^* \rangle_{L^2} \\
-\dot{p}_2 q_1^2 \langle \zeta_{1x_2}, \boldsymbol{\phi}_2^* \rangle_{L^2} - \dot{p}_1 q_1 q_2 \langle \zeta_{3x_1}, \boldsymbol{\phi}_2^* \rangle_{L^2} - \dot{p}_2 \eta \langle \zeta_{4x_2}, \boldsymbol{\phi}_2^* \rangle_{L^2}, \\
\langle \mathcal{L}(\boldsymbol{U}), \boldsymbol{\phi}_2^* \rangle_{L^2} = \left( \frac{1}{6} \langle F'''(S) \boldsymbol{\psi}_2{}^3, \boldsymbol{\phi}_2^* \rangle_{L^2} + \langle F''(S) \boldsymbol{\psi}_2 \zeta_2, \boldsymbol{\phi}_2^* \rangle_{L^2} \right) q_2^3 \\
+ \left( \frac{1}{2} \langle F'''(S) \boldsymbol{\psi}_1^2 \boldsymbol{\psi}_1, \boldsymbol{\phi}_2^* \rangle_{L^2} + \langle F''(S) \boldsymbol{\psi}_2 \zeta_1, \boldsymbol{\phi}_2^* \rangle_{L^2} + \langle F''(S) \boldsymbol{\psi}_1 \zeta_3, \boldsymbol{\phi}_2^* \rangle_{L^2} \right) q_1^2 q_2 \\
+ \eta \left( \langle F''(S) \boldsymbol{\psi}_2 \zeta_4, \boldsymbol{\phi}_2^* \rangle_{L^2} + \langle \boldsymbol{g}'(S) \boldsymbol{\psi}_2, \boldsymbol{\phi}_2^* \rangle_{L^2} \right) q_2.
\end{cases} \tag{7.2}
$$

We know that $\dot{p}_1 = q_1$ and $\dot{p}_2 = q_2$ from the inner products with $\boldsymbol{\psi}_1^*$ and $\boldsymbol{\psi}_2^*$, respectively. Here we show only nonzero terms.

In what follows we calculate each term of (7.1) and (7.2). Since $\boldsymbol{\psi}_1 = \cos\theta\psi(r)$ and $\boldsymbol{\phi}_1 = \cos\theta\phi(r)$ and so on, the first term is given as

$$\frac{1}{6}\langle F'''(S)\boldsymbol{\psi}_1^3, \boldsymbol{\phi}_1^*\rangle_{L^2} = \frac{\pi}{8}\int_0^\infty r\langle F'''(S)\psi^3, \phi^*\rangle \mathrm{d}r.$$

By similar calculations to the above, we have

$$\begin{aligned}\frac{1}{6}\langle F'''(S)\boldsymbol{\psi}_1^3, \boldsymbol{\phi}_1^*\rangle_{L^2} &= \frac{1}{2}\langle F'''(S)\boldsymbol{\psi}_1{\boldsymbol{\psi}_2}^2, \boldsymbol{\phi}_1^*\rangle_{L^2} \\ = \frac{1}{6}\langle F'''(S)\boldsymbol{\psi}_2^3, \boldsymbol{\phi}_2^*\rangle_{L^2} &= \frac{1}{2}\langle F'''(S)\boldsymbol{\psi}_1^2\boldsymbol{\psi}_2, \boldsymbol{\phi}_2^*\rangle_{L^2}.\end{aligned}$$

We can rewrite (4.5) as

$$\begin{cases} -L\zeta_1 = \dfrac{1}{2}F''(S)\cos^2\theta\psi^2 + \cos^2\theta\psi_r + \dfrac{\sin^2\theta}{r}\psi, \\ -L\zeta_2 = \dfrac{1}{2}F''(S)\sin^2\theta\psi^2 + \sin^2\theta\psi_r + \dfrac{\cos^2\theta}{r}\psi, \\ -L\zeta_3 = \dfrac{1}{2}\sin 2\theta\left(F''(S)\psi^2 + 2\left(\psi_r - \dfrac{\psi}{r}\right)\right), \\ -L\zeta_4 = \boldsymbol{g}(S). \end{cases}$$

The term of $\zeta^* \equiv \zeta_1 - \zeta_2$ satisfies

$$\begin{aligned}-L\zeta^* &= \frac{1}{2}(\cos^2\theta - \sin^2\theta)\left(F''(S)\psi^2 + 2\left(\psi_r - \frac{\psi}{r}\right)\right) \\ &= \frac{1}{2}\sin\left(2\theta + \frac{\pi}{2}\right)\left(F''(S)\psi^2 + 2\left(\psi_r - \frac{\psi}{r}\right)\right).\end{aligned}$$

Hence we have $\zeta^*(r,\theta) = \zeta_3\left(r, \theta + \pi/4\right)$.

We note that $\zeta_1 = \cos^2\theta\tilde{\zeta_1}(r) + \sin^2\theta\tilde{\zeta_2}(r)$, $\zeta_2 = \sin^2\theta\tilde{\zeta_1}(r) + \cos^2\theta\tilde{\zeta_2}(r)$, $\zeta_3 = \sin 2\theta\tilde{\zeta_3}(r)$ holds and $\zeta_4$ is radially symmetric as $\zeta_4 = \tilde{\zeta_4}(r)$. It is easy to see that $\zeta_2(r,\theta) = \zeta_1\left(r, \theta + \pi/2\right)$. Therefore, we show

$$\langle F''(S)\boldsymbol{\psi}_1\zeta_1, \boldsymbol{\phi}_1^*\rangle_{L^2} = \frac{3\pi}{4}\int_0^\infty r\langle F''\psi\tilde{\zeta_1}, \phi^*\rangle \mathrm{d}r + \frac{\pi}{4}\int_0^\infty r\langle F''\psi\tilde{\zeta_2}, \phi^*\rangle \mathrm{d}r.$$

Similarly, we have

$$\begin{aligned}\langle F''(S)\boldsymbol{\psi}_1\zeta_1, \boldsymbol{\phi}_1^*\rangle_{L^2} &= \langle F''(S)\boldsymbol{\psi}_1\zeta_2, \boldsymbol{\phi}_1^*\rangle_{L^2} + \langle F''(S)\boldsymbol{\psi}_2\zeta_3, \boldsymbol{\phi}_1^*\rangle_{L^2} \\ = \langle F''(S)\boldsymbol{\psi}_2\zeta_2, \boldsymbol{\phi}_2^*\rangle_{L^2} &= \langle F''(S)\boldsymbol{\psi}_2\zeta_1, \boldsymbol{\phi}_2^*\rangle_{L^2} + \langle F''(S)\boldsymbol{\psi}_1\zeta_3, \boldsymbol{\phi}_2^*\rangle_{L^2}.\end{aligned}$$

Here we use the relation of $\tilde{\zeta}^*(r) = \tilde{\zeta_1}(r) - \tilde{\zeta_2}(r) = \tilde{\zeta_3}(r)$.

The last term to constant $M_1$ is obtained as

$$\langle \zeta_{1x_1}, \boldsymbol{\phi}_1^* \rangle_{L^2} = \frac{3\pi}{4} \int_0^\infty r \langle \tilde{\zeta}_{1r}, \phi^* \rangle \mathrm{d}r + \frac{\pi}{4} \int_0^\infty r \langle \tilde{\zeta}_{2r}, \phi^* \rangle \mathrm{d}r - \frac{\pi}{2} \int_0^\infty \langle \tilde{\zeta}^*, \phi^* \rangle \mathrm{d}r.$$

Here, we also obtain

$$\begin{aligned} &\langle \zeta_{1x_1}, \boldsymbol{\phi}_1^* \rangle_{L^2} - \langle \zeta_{2x_1}, \boldsymbol{\phi}_1^* \rangle_{L^2} - \langle \zeta_{3x_2}, \boldsymbol{\phi}_1^* \rangle_{L^2} \\ =& \frac{\pi}{2} \int_0^\infty r \langle \tilde{\zeta}_{1r}, \phi^* \rangle \mathrm{d}r - \frac{\pi}{2} \int_0^\infty r \langle \tilde{\zeta}_{2r}, \phi^* \rangle \mathrm{d}r + \pi \int_0^\infty r \langle \tilde{\zeta}^*, \phi^* \rangle \mathrm{d}r \\ &- \frac{\pi}{2} \int_0^\infty r \langle \tilde{\zeta}_{3r}, \phi^* \rangle \mathrm{d}r - \pi \int_0^\infty r \langle \tilde{\zeta}_3, \phi^* \rangle \mathrm{d}r = 0. \end{aligned}$$

By comparing above results, we have

$$\begin{aligned} \langle \zeta_{1x_1}, \boldsymbol{\phi}_1^* \rangle_{L^2} =& \langle \zeta_{2x_1}, \boldsymbol{\phi}_1^* \rangle_{L^2} + \langle \zeta_{3x_2}, \boldsymbol{\phi}_1^* \rangle_{L^2} \\ = \langle \zeta_{2x_2}, \boldsymbol{\phi}_2^* \rangle_{L^2} =& \langle \zeta_{1x_2}, \boldsymbol{\phi}_2^* \rangle_{L^2} + \langle \zeta_{3x_1}, \boldsymbol{\phi}_2^* \rangle_{L^2}. \end{aligned}$$

Others are shown quite similarly as

$$\begin{aligned} &\langle F''(S)\boldsymbol{\psi}_1\zeta_4, \boldsymbol{\phi}_1^* \rangle_{L^2} + \langle \boldsymbol{g}'(S)\boldsymbol{\psi}_1, \boldsymbol{\phi}_1^* \rangle_{L^2} \\ =& \pi \int_0^\infty r \langle F''(S)\psi\tilde{\zeta}_4, \phi^* \rangle \mathrm{d}r + \pi \int_0^\infty r \langle \boldsymbol{g}'(S)\psi, \phi^* \rangle \mathrm{d}r \\ =& \langle F''(S)\boldsymbol{\psi}_2\zeta_4, \boldsymbol{\phi}_2^* \rangle_{L^2} + \langle \boldsymbol{g}'(S)\boldsymbol{\psi}_2, \boldsymbol{\phi}_2^* \rangle_{L^2}. \end{aligned}$$

The last term to $M_2$ is obtained as

$$\langle \zeta_{4x_1}, \boldsymbol{\phi}_1^* \rangle_{L^2} = \pi \int_0^\infty r \langle \tilde{\zeta}_{4r}, \phi^* \rangle \mathrm{d}r = \langle \zeta_{4x_2}, \boldsymbol{\phi}_2^* \rangle_{L^2}.$$

Substituting the results into (7.1) and (7.2), we arrive at (4.6) and (4.7).

## References


[1] Batiste, O., Knobloch, E., Alonso, A., and Mercader, I., Spatially localized binary-fluid convection, *J. Fluid Mech.*, **560** (2006), 149–158.

[2] Bode, M., Liehr, A. W., Schenk, C. P., and Purwins, H.-G., Interaction of dissipative solitons: particle-like behaviour of localized structures in a three-diffusion system, *Physica D*, **161** (2002), 45–66.

[3] Burke, J. and Knobloch, E., Localized states in the generalized Swift-Hohenberg equation, *Phys. Rev. E*, **73** (2006), 056211.

[4] de Kepper, P., Perraud, J. J., Rudovics, B., and Dulos, E., Experimental study of stationary Turing patterns and their interaction with traveling waves in a chemical system, *Int. J. Bifurcation Chaos Appl. Sci. Eng.*, **4** (1994), 1215–1231.

[5] Doelman, A., Eckhaus, W., and Kaper, T.J., Slowly modulated two-pulse solutions in the Gray.Scott model II: geometric theory, bifurcations, and splitting dynamics, *SIAM J. Appl. Math.*, **61** (2001), 2036–2062.
[6] Ei, S.-I., Mimura, M., and Nagayama, M., Interacting spots in reaction diffusion systems, *Discrete Contin. Dyn. Syst.*, **14** (2006), 31–62.
[7] Gray, P., and Scott, S. K., Autocatalytic reactions in the isothermal, continuous stirred tank reactor: oscillations and instabilities in the system A + 2B → 3B, B→C, *Chem. Eng. Sci.*, **39** (1984), 1087–1097.
[8] Iima, M., and Nishiura, Y., Unstable periodic solution controlling collision of localized convection cells in binary fluid mixture, *Physica D*, **238** (2009), 449–460.
[9] Lee, K. J., McCormick, Q. D., Pearson, J. E., and Swinney, H. L., Experimental observation of self-replicating spots in a reaction-diffusion system, *Nature*, **369** (1994), 215–218.
[10] Kobayashi, R., Hayase, Y., and Ohta, T., Self-organized pulse generator, *Physica D*, **84** (1995), 162–170.
[11] Kolodner, P., Collisions between pulses of traveling-wave convection, *Phys. Rev. A*, **44** (1991), 6466–6479.
[12] Kolodner, P., Glazier, J. A., and Williams, H., Dispersive chaos in one-dimensional traveling-wave convection, *Phys. Rev. Lett.*, **65** (1990), 1579–1582.
[13] Kolokolnikov, T., Ward, M. J., and Wei, J., The existence and stability of spike equilibria in the one-dimensional Gray.Scott model: the pulse-splitting regime, *Physica D*, **202** (2005), 258–293.
[14] Meinhardt, H., The Algorithmic of Beauty of Sea Shells, Springer (1995).
[15] Nagai, K., Sumino, Y., Kitahata, H., and Yoshikawa, K., Mode selection in the spontaneous motion of an alcohol droplet, *Phys. Rev. E*, **71** (2005), 065301.
[16] Nettesheim, S., von Oertzen, A., and Rotermund, H., H., and Ertl, G., Reaction diffusion patterns in the catalytic CO-oxidation on Pt(110): Front propagation and spiral waves, *J. Chem. Phys.*, **98** (1993), 9977.
[17] Nishiura, Y., Far-from-equilibrium Dynamics, *Translations of Mathematical Monographs* **209**, (AMS, 2002).
[18] Nishiura, Y., Oyama, Y., and Ueda, K.-I., Dynamics of traveling pulses in heterogeneous-media of jump type, *Hokkaido Math. J.*, **36** (2007), 207–242.
[19] Nishiura, Y., and Teramoto, T., Collision dynamics in dissipative systems, *Theor. Appl. Mech. Japan*, **59** (2010), 13–25.
[20] Nishiura, Y., Teramoto, T., and Ueda, K.-I., Scattering and separators in dissipative systems, *Phys. Rev. E*, **67** (2003), 056210.
[21] Nishiura, Y., Teramoto, T., and Ueda, K.-I., Dynamics transitions through scattors in dissipative systems, *Chaos*, **13** (2003), 962–972.
[22] Nishiura, Y., Teramoto, T., and Ueda, K.-I., Scattering of traveling spots in dissipative systems, *Chaos*, **15** (2005), 047509.
[23] Nishiura, Y., Teramoto, T., and Yadome, M., Heterogeneity-induced pulse generators, to appear in the proceedings of the 3rd International Conference on Cognitive Neurodynamics (ICCN2011).
[24] Nishiura, Y., Teramoto, T., and Yuan, X., Heterogeneity-induced spot dynamics for three-component reaction-diffusion systems, *Commun. Pure Appl. Anal.*, **11** (2011), pp. 307–338
[25] Nishiura, Y., Teramoto, T., Yuan, X., and Ueda, K.-I., Dynamics of traveling pulses in heterogeneous media, *Chaos*, **17** (2007), 037104.
[26] Nishiura, Y., and Ueyama, D., A skeleton structure of self-replicating dynamics, *Physica*

*D*, **130** (1999), 73–104.
[27] Nishiura, Y., and Ueyama, D., Spatial-temporal chaos in Gray-Scott model, *Physica D*, **150** (2001), 137–162.
[28] Pauwelussen, J. P., Nerve impulse propagation in a branching nerve system: a simple model, *Physica D*, **4** (1981), 67–88.
[29] Pearson., J. E., Complex patterns in a simple system, *Science*, **216** (1993), 189–192.
[30] Prat, A., Li, Y.-X., and Bressloff, P., Inhomogeneity-induced bifurcation of stationary and oscillatory pulses, *Physica D*, **202** (2005), 177–199.
[31] Purwins, H.-G., Bödeker, H. U., and Amiranashvili, S., Dissipative solitons, *Advances in Physics*, **59** (2010), 485–701.
[32] Rotermund, H. H., Jakubith, S., von Oertzen, A., and Ertl, G., Solitons in a surface reaction, *Phys. Rev. Lett.*, **66** (1991), 3083–3086.
[33] Steele, A. J., Tinsley, M., and Showalter, K., Collective behavior of stabilized reaction-diffusion waves, *Chaos*, **18** (2008), 026108.
[34] Takagi, S., Nishiura, Y., Nakagaki, T., Ueda, T., and Ueda, K.-I., Indecisive behavior of amoeba crossing an environmental barrier, *Proc. Int. Symp. On Topological Aspects of Critical Systems and Networks*, 86–93.
[35] Teramoto, T., Ueda, K.-I., and Nishiura, Y., Phase-dependent output of scattering process for traveling breathers, *Phys. Rev. E*, **69** (2004), 056224.
[36] Teramoto, T., Yuan, X., Bär, and Nishiura, Y., Onset of unidirectional pulse propagation in an excitable medium with asymmetric heterogeneity, *Phys. Rev. E*, **79** (2009), 046205.
[37] Teramoto, T., Suzuki, K., and Nishiura, Y., Rotational motion of traveling spots in dissipative systems, *Phys. Rev. E*, **80** (2009), 046208.
[38] Teramoto, T., and Nishiura Y., Traveling Spots Through a Line of Heterogeneity, *preprint.*
[39] Toyota, T., Maru, N., Hanczyc, M., M., Ikegami, T., and Sugawara, T., Self-Propelled Oil Droplet Consuming Fuel Surfactant, *J. Am. Chem. Soc.*, **13** (2009), 5012–5013.
[40] Ueda, K., Takagi, S., Nishiura, Y., and Nakagaki, T., Mathematical model for contemplative amoeboid locomotion, *Phys. Rev. E*, **83** (2011), 021916.
[41] Umbanhowar, P. B., Melo, F., and Swinney, H. L., Localized excitations in a vertically vibrated granular layer, *Nature*, **382** (1996), 793–796.
[42] Vanag, V. K., and Epstein, I. R., Localized patterns in reaction-diffusion systems, *Chaos*, **17** (2007), 037110.
[43] Yuan, X., Teramoto, T., and Nishiura, Y., Heterogeneity-induced defect bifurcation and pulse dynamicsfor a three-component reaction-diffusion system, *Phys. Rev. E*, **75** (2007), 036220.
[44] van Heijster, P., and Sandstede, B., Planar radial spots in a three-component FitzHugh-Nagumo system, *J. Nonlinear Sci.*, **21** (2011), 705–745.
[45] Waddington, C. H., The Strategy of the Genes, (Allen & Unwin, 1957).
[46] Zhabotinsky, A. M., Eager, M. D., and Epstein, I. R., Refraction and reflection of chemical waves, *Phys. Rev. Lett.*, **71** (1993), 1526–1529.